

**Initial-value-problem solution for isolated rippled shock fronts in arbitrary fluid media**

Jason W. Bates\*

*Plasma Physics Division, U.S. Naval Research Laboratory, Washington, D.C. 20375, USA*

(Received 1 October 2003; published 28 May 2004)

Following the work of Roberts [Los Alamos Scientific Laboratory Report No. LA-299, 1945 (unpublished)], we investigate the effect of small two-dimensional perturbations on an isolated, planar shock front moving steadily through an inviscid fluid medium with an arbitrary equation of state (EOS). In the context of an initial-value problem, we derive explicit analytical expressions for the linearized, time-dependent Fourier coefficients associated with an initial corrugation of the front. The temporal evolution of these coefficients superficially resembles the attenuated “ringing” of a damped harmonic oscillator, but with the important distinctions that the frequency of oscillation is not constant, and that the damping factor is not simply an exponential function of time  $t$ . It is shown that at least two three-parameter families of stable solutions exist, one more strongly damped than the other. In both cases, we find that the envelope of oscillations decays asymptotically as  $t^{-3/2}$ , with shorter wavelengths dying out earlier than longer ones. For a particular perturbed-shock system, the strength of the front and the EOS properties of the material through which it propagates determine the applicable family of solutions. Theoretical predictions agree well with FAST2D numerical simulations for several examples derived from the CALEOS library.

DOI: 10.1103/PhysRevE.69.056313

PACS number(s): 47.40.-x, 51.30.+i, 47.20.-k

**I. INTRODUCTION**

Shock waves are ubiquitous in compressible hydrodynamic systems ranging from interstellar media [1] to traffic flow [2]. Of fundamental importance to the dynamics of shock waves is an understanding of how disturbances to otherwise steady shock fronts evolve in time. The earliest analysis of this problem is likely due to Roberts [3], who considered the effect of small perturbations on isolated planar shocks propagating through homogeneous fluids from the point of view of an initial-value problem. The use of the word “isolated” here implies that a shock is very far, or “decoupled,” from its driving mechanism (e.g., a moving piston). Working in the context of an ideal fluid description, Roberts reduced the linearized system of governing equations to an integral expression, the evaluation of which yields the time-dependent amplitude of each Fourier component of the initial disturbance. His work demonstrated that shocks are almost always stable, with perturbations decaying asymptotically in time  $t$  at least as fast as  $t^{-1/2}$ . One obvious oversight of Roberts’ analysis, though, is that the presence of entropy perturbations behind the shock is neglected; moreover, results are specialized to the case of a perfect gas.

In this paper, we generalize Roberts’ calculation and derive explicit expressions governing the temporal evolution of a rippled shock front in a fluid medium with an arbitrary equation of state (EOS). The solution methodology is based on a perturbative expansion, with the ratio of shock-ripple amplitude to wavelength serving as a small parameter. Information about the EOS of a specific material is contained in three dimensionless parameters that characterize the unperturbed shock, and serve as necessary inputs for the first-order theory. The three parameters, which in this study are derived from the CALEOS library [4] at the U.S. Naval Research

Laboratory (NRL), are the D’yakov parameter  $h$  (a quantity that is inversely proportional to the slope of the shock Hugoniot [5]), the compression ratio  $\eta$ , and the Mach number behind the shock,  $M_1$ . Several examples are considered in our analysis that underscore a somewhat unexpected result. It is shown that at least two families of damped oscillatory solutions exist for initial disturbances localized at the shock front. The determination of which family applies to a particular perturbed-shock system depends on the sign of a certain dimensionless quantity  $\Lambda$ , which is an algebraic function of the three shock parameters  $h$ ,  $\eta$ , and  $M_1$  only. The properties of the two families of solutions are similar in that they share the same late-time asymptotic behavior (oscillations decay in time as  $t^{-3/2}$ ), but differ in the degree of damping that the oscillations experience initially; see Fig. 1. All ideal gases belong to the family of solutions with  $\Lambda > 0$ . For moderately strong shocks in materials such as polystyrene, aluminum, and deuterium-tritium “ice,” the parameter  $\Lambda$  is negative (according to the CALEOS database), and the behavior is accurately described by the more strongly damped family of solutions. At sufficiently large driving pressures, though, the sign of  $\Lambda$  eventually becomes positive—the threshold for this continuous crossover being material dependent.

The motivation for this study is borne out of an interest to understand better the implosion of inertial confinement fusion (ICF) targets, which contain materials whose equations of state are far from ideal [6]. In most ICF schemes, it is required to compress fuel pellets containing mixtures of deuterium and tritium to densities as much as 1000 times greater than solid values [7]. The compression of the fuel results from multiple shock waves launched into the pellet by high-intensity radiation striking its surface and ablating away the outermost layers of material. Successful compression requires that the ablation and compression processes occur with near-perfect symmetry, otherwise high fusion-reaction yield may not be achieved [8]. Asymmetric irradiation and/or rough surface finishes can lead to a nonuniform ablation pro-

\*FAX: (202)767-0046; Email address: bates@this.nrl.navy.mil

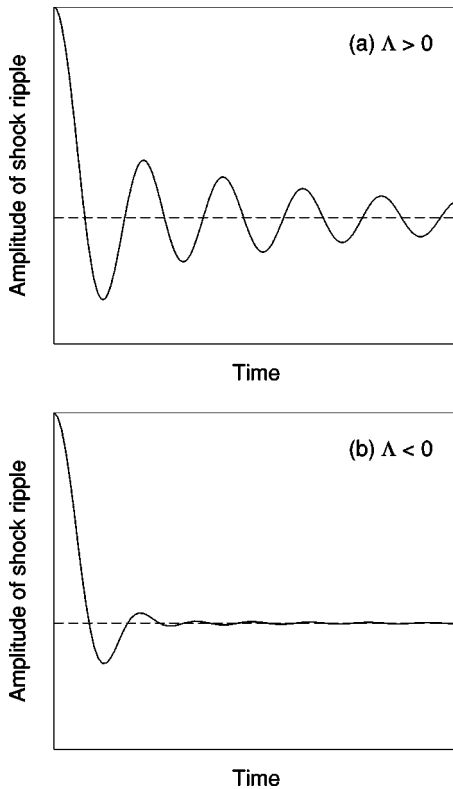


FIG. 1. Qualitative difference between the two families of solutions for an isolated, rippled shock wave. Although the amplitudes of shock ripples decay asymptotically in both cases as  $t^{-3/2}$ , the degree of initial damping in one family is typically smaller than in the other. The lesser-damped example shown in (a) corresponds to a positive value of the parameter  $\Lambda$  [defined in Eq. (55)], whereas in (b),  $\Lambda$  is negative.

cess, and thus to the generation of perturbed shock waves. The presence of distorted fronts in ICF pellets is significant because of their potential for seeding hydrodynamic instabilities (via “interface imprinting” [9] or otherwise [10]), which disturb uniform high-density compression and reduce gain. A better understanding of the dynamics of perturbed shocks in real materials could provide insight into how to suppress these instabilities, thus improving the overall uniformity of the compression process.

Previous work by Ishizaki and Nishihara [11] has explored the subject of perturbed shocks generated by nonuniform ablation surfaces in planar ICF targets. The authors were able to solve for the time history of the rippled shock and ablation fronts, and demonstrate fair agreement with experiments [12], but their theoretical model relied on a perfect-gas EOS with an artificially large value for the ratio of specific heats. In the present study, we do not attempt to model the complete ICF-compression scenario, but rather focus our efforts on assessing the influence that real equations of state have on the dynamics of perturbed-shocks. Although the issue of how such perturbations might arise physically is not addressed by the theory, we expect that the solution contained herein will contribute to a more complete understanding of the shock-compression process in ICF. Moreover, the solution may have direct relevance to other perturbed-shock

problems in gas dynamics as well. Fraley [13], for example, has shown that isolated rippled shocks possess many of the same general properties as those generated by curved pistons [14,15], or reflected from corrugated walls [16].

As it stands, the isolated rippled-shock solution presented in this paper also serves as a useful benchmark for hydrodynamic-based computer codes used in ICF research. Modern ICF codes usually comprise a sequence of distinct “modules” for simulating various physical phenomena such as hydrodynamic motion, thermal conduction, and radiation transport, as well as accounting for realistic EOS information (often through a table look-up procedure) [17–21]. The only way to verify the fidelity of such complicated codes is through the use of limiting test cases that are amenable to analytical solutions. Presently, however, very few analytically tractable problems relevant to hydrodynamic stability calculations are available—Rayleigh-Taylor [22] and Richtmeyer-Meshkov [23] problems being the only other known examples. The isolated rippled-shock problem thus provides a valuable addition to the suite of available “reality checks” for testing and debugging numerical simulations. This subject has been discussed previously by Munro [24], who used the analytical solution of a rippled-shock problem to check the accuracy of the code LASNEX [17], but found rather poor agreement. In contrast, it will be shown here that the FAST2D code [18,21] (with the thermal conduction and radiation transport modules disabled) performed well on the isolated rippled-shock problem; simulation results show excellent agreement with theoretical predictions for the evolution of shock-ripple amplitudes.

This paper is organized as follows. In Sec. II, we formulate the initial-value problem for the isolated perturbed-shock system, and derive the governing first-order equations, as well as the linearized boundary conditions that they must obey. In Sec. III, these equations are reduced to an integral expression for the time-dependent shock-ripple amplitude. (Up to this stage, our approach closely follows that of Roberts, but with the important distinctions that the present analysis accounts for the existence of postshock entropy-vortex waves, and non-ideal-gas equations of state.) Section IV outlines the solution of the integral equation via Laplace transforms, which involves one of two different inversion procedures, depending on the sign of the quantity  $\Lambda$ . Comparisons of results from numerical simulations using the FAST2D code in conjunction with the CALEOS database appear in Sec. V. Finally in Sec. VI, the conclusions of the paper are given. For convenience, Laplace transforms and other mathematical relations that were useful in this investigation are listed in the Appendix.

## II. FORMULATION OF THE INITIAL-VALUE PROBLEM

The first step in our analysis is to define the “zeroth-order” state upon which perturbations are to be imposed. We choose this to be a one-dimensional, planar step shock moving in the laboratory frame with a constant speed  $D$ . The shock propagates into a half-space filled by a fluid medium at rest with density  $\rho_0$ , pressure  $p_0$ , and entropy per unit mass  $s_0$ . Behind the unperturbed shock, the density, pres-

sure, and specific entropy have the values  $\rho_1$ ,  $p_1$ , and  $s_1$ , respectively. We imagine that a steadily moving driving mechanism (such as a piston or ablation front) supports the shock from behind, but that its influence on the shock dynamics is negligible. That is, we assume that the shock is far enough away from the driving mechanism that the transit time of a sound wave between the two surfaces is much longer than the time of interest for this problem.

The unperturbed state  $(\rho_1, p_1)$  is, of course, not arbitrary, but constrained to lie on the principal Hugoniot curve, which is the locus of all compressed, or “downstream,” states that can be realized behind a single shock front given the initial, or “upstream,” condition  $(\rho_0, p_0)$ . The shape and other important geometric properties of this curve are greatly influenced by the EOS of the substance through which the shock propagates [25]. In the case of a perfect gas, the equation for the Hugoniot can be calculated analytically, with the result expressible in a simple closed form. For nonideal materials, the situation is slightly more involved in that an accurate calculation of the Hugoniot usually requires the use of complex EOS models to supply realistic thermodynamic data. Examples of such models include CALEOS [4], SESAME [26], and QEOS [27], all of which characterize a variety of substances over a wide range of pressure and density states by combining theoretical, empirical, and phenomenological descriptions [6]. A few Hugoniots derived from the CALEOS database are presented in Fig. 2 for materials of interest to ICF research. For comparison, these figures also show the corresponding results for the more widely used SESAME library. As Fig. 2 demonstrates, the theoretical predictions of different EOS models for the same material are not always in agreement, but we shall not attempt to address these discrepancies here since such a discussion lies beyond the scope of the present investigation. In the analysis that follows, we shall employ the CALEOS model exclusively to characterize the properties of shock waves in materials with nonideal equations of state.

A quantity that plays an important role in the study of perturbed shocks is the slope of the Hugoniot curve in the plane of density  $\rho$  versus pressure  $p$ . Note that this slope—which is written as  $(dp/d\rho)_H$  and evaluated at the downstream state—is distinct from the postshock isentropic derivative,  $(\partial p/\partial \rho)_s = c^2$ . Here, the subscript  $s$  implies constant entropy and  $c$  is the speed of sound in the compressed fluid. Although these two derivatives possess a second-order tangency at the initial state, and are approximately equal for weak shock waves [29], they can differ appreciably even for moderately strong shocks. A useful way of expressing the (inverse) slope of the Hugoniot is in terms of the dimensionless “D’yakov parameter” [5]

$$h = -\frac{j^2}{\rho_1^2} \left( \frac{d\rho}{dp} \right)_H, \quad (1)$$

where  $j = \rho_0 D$  is the mass flux density across the shock. According to a linearized normal-mode analysis [5,30,31], stable shocks obey the condition

$$-1 < h < 1 + 2M_1, \quad (2)$$

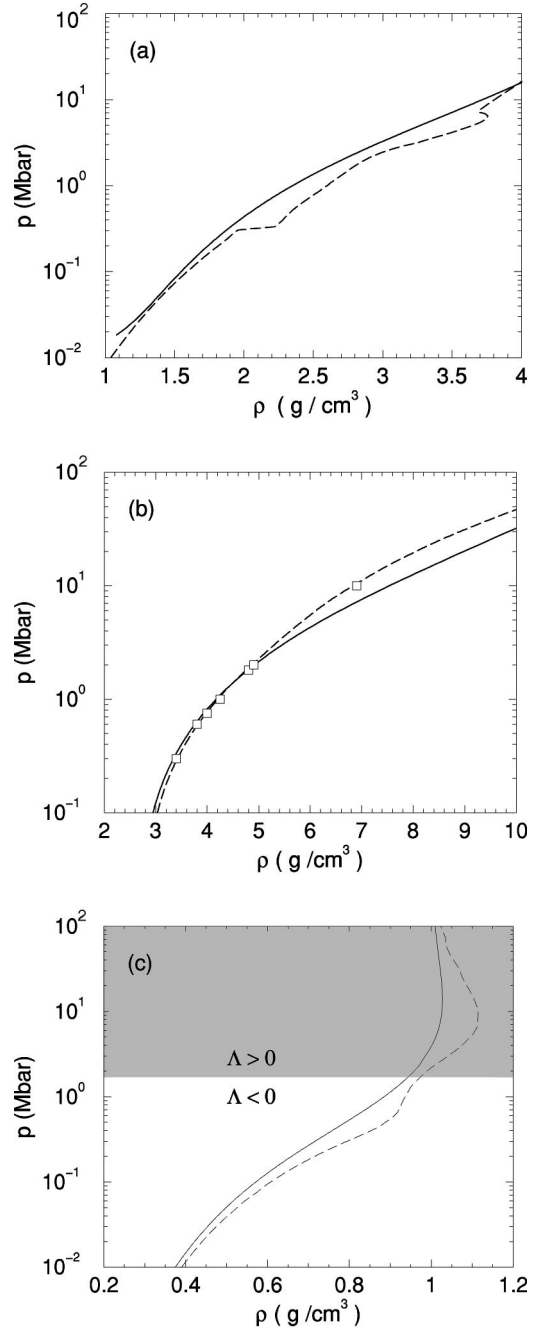


FIG. 2. Examples of Hugoniot curves for (a) polystyrene, (b) aluminum, and (c) deuterium-tritium ice. Solid and dashed curves show results derived from the CALEOS and SESAME EOS libraries, respectively. The symbols in (b) are experimental data points taken from Ref. [28]. According to CALEOS, the sign of  $\Lambda$  in (c) changes from negative to positive near  $p_1 = 1.7$  Mbar, indicating a transition to a lesser-damped solution above that value (shaded region). For the range of density values in (a) and (b), the sign of  $\Lambda$  is strictly negative.

where  $M_1 = (D - U)/c$  is a downstream Mach number satisfying  $0 < M_1 < 1$  and  $U$  is the mass velocity of the shocked fluid in the laboratory reference frame. Planar shocks in materials with values of  $h$  that lie outside of this range experience exponential growth of perturbations [25,32], and are

thus unstable. In Eq. (2), the lower limit is known to correspond to the breakup of a shock into two waves traveling in the same direction [33], and has long been observed experimentally in substances undergoing phase transformations, or yielding plastically at the elastic limit [34]. Satisfaction of the condition  $1+2M_1 < h$ , on the other hand, has been shown by Gardner [35] to correspond to the splitting of a shock into two counterpropagating waves, although this phenomenon apparently lacks experimental confirmation. For the examples considered in this study, all values of  $h$  lie well within the stability limits specified by Eq. (2).

Let us proceed with our perturbative analysis of the isolated rippled-shock problem. In anticipation of the linearization procedure to follow, it is convenient at this stage to transform our frame of reference to one in which the unperturbed compressed fluid behind the shock front is stationary. In such a reference frame, the unperturbed planar shock moves with speed  $D-U$ , the upstream fluid flows at speed  $U$ , and the normal and transverse components of the unperturbed velocity field behind the shock front vanish. This arrangement is advantageous because it reduces the complexity of the first-order algebraic expressions significantly. By applying the law of mass conservation, one can easily show that

$$D-U = D/\eta, \quad (3)$$

where  $\eta = \rho_1/\rho_0$  and  $D > U$ . Additionally, conservation of momentum requires

$$p_1 = p_0 + \rho_1 D^2 (\eta - 1) / \eta^2. \quad (4)$$

Equations (3) and (4) are two of the three well-known conservation laws for planar shocks known as the Rankine-Hugoniot relations [29]. The missing equation, which expresses conservation of energy, does not play a direct role in the present analysis.

Next, we wish to derive an expression for the position of the propagating shock front. To do so, we let  $x$  be the coordinate normal to the undisturbed planar front and  $y$  the coordinate along it, as shown in Fig. 3. Assuming that the shock moves in the negative  $x$  direction, its unperturbed position as a function of time is given by  $x + (D-U)t = 0$ . We now introduce first-order perturbations into the shape of the front, and in the hydrodynamic quantities behind it. In general, such a disturbance will give rise to two types of waves in the downstream flow: entropy-vortex and sound waves [25]. Since these waves carry energy away from the front whose distortion is the ultimate source of the perturbation, we may expect that it will eventually regain its planarity, even in the absence of transport coefficients such as viscosity and thermal conduction [36]. For a single-mode perturbation with wave number  $k$  and amplitude  $\delta x(t)$ , the position of the perturbed shock is

$$x_s(y,t) = -(D-U)t + \delta x(t) e^{iky}, \quad (5)$$

where  $i = \sqrt{-1}$ , and the real part of the right-hand side of this equation is implied. Note that to account for an arbitrary multimode perturbation to the shock front,  $\delta x$  in Eq. (5)

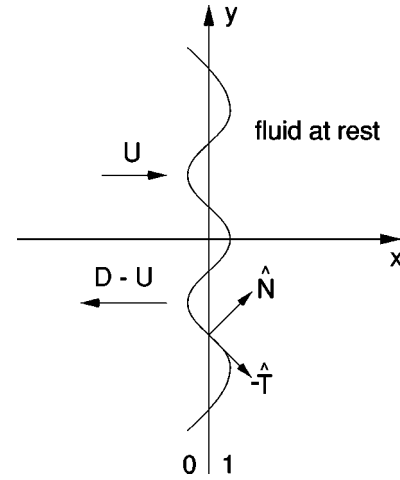


FIG. 3. Geometry of an isolated, rippled shock front in the frame of reference in which the downstream fluid is at rest. The unperturbed planar shock moves in the negative  $x$  direction with velocity  $-(D-U)\hat{x}$ , while the upstream fluid flows at velocity  $U\hat{x}$ . Unit vectors normal and tangential to the rippled front are denoted by  $\hat{N}$  and  $\hat{T}$ , respectively.

should be replaced with the indexed coefficient  $\delta x_k$ , and a summation over all  $k$  values in the spectrum performed. (A similar Fourier decomposition would apply to the hydrodynamic quantities to be introduced shortly.) Owing to the linear independence of the functions  $\exp(iky)$ , though, the result of this procedure is merely a single set of relations that must be satisfied for every value of  $k$ , and is identical to that obtained using the single-mode formulation above. For this reason, we shall avoid the additional notational complexity associated with a formal superposition of Fourier modes, and limit our analysis to a single  $k$  value only. The final expressions that we derive can then be easily generalized to treat multi-mode perturbation as the need arises. We should also point out that the amplitude  $\delta x(t)$  in Eq. (5) is considered to be a “small” quantity—a statement that will be made more precise momentarily. Furthermore, note that at this stage the functional dependence of  $\delta x(t)$  is unconstrained; we have not assumed, for instance, that it has the “normal-mode” form  $\exp(-i\omega t)$ , where the frequency  $\omega$  would be related to  $k$  through a dispersion relation.

Since the zeroth-order flow is stationary in the shocked-gas reference frame, we can write the postshock normal and transverse components of the flow velocity as

$$u_x(x,y,t) = \delta u_x(x,t) e^{iky}, \quad (6)$$

$$u_y(x,y,t) = \delta u_y(x,t) e^{iky}, \quad (7)$$

respectively. Similarly, the pressure, density, and specific entropy behind the shock are

$$p(x,y,t) = p_1 + \delta p(x,t) e^{iky}, \quad (8)$$

$$\rho(x,y,t) = \rho_1 + \delta \rho(x,t) e^{iky}, \quad (9)$$

$$s(x,y) = s_1 + \delta s(x) e^{iky}. \quad (10)$$

In Eqs. (8)–(10), a quantity prefixed by a  $\delta$  denotes the amplitude of a hydrodynamic perturbation whose magnitude is assumed to be much smaller than its zeroth-order counterpart (e.g.,  $\delta p \ll p_1$ ). Note that in the shocked-gas reference frame, the entropy perturbation  $\delta s$  is independent of time. This is a consequence of the fact that entropy-vortex waves behind a shock propagate with the zeroth-order, downstream fluid velocity, which has zero magnitude here.

Let us determine the first-order equations describing hydrodynamic motion behind the perturbed shock front. The governing expressions are the Euler equations for isentropic flow:

$$\frac{\partial \rho}{\partial t} + \nabla \cdot (\rho \mathbf{u}) = 0, \quad (11)$$

$$\rho \frac{\partial \mathbf{u}}{\partial t} + \rho(\mathbf{u} \cdot \nabla) \mathbf{u} = -\nabla p, \quad (12)$$

$$\frac{\partial s}{\partial t} + \mathbf{u} \cdot \nabla s = 0. \quad (13)$$

Here, the fluid velocity  $\mathbf{u}$  is given by  $u_x \hat{\mathbf{x}} + u_y \hat{\mathbf{y}}$ , where  $\hat{\mathbf{x}}$  and  $\hat{\mathbf{y}}$  are unit vectors in the  $x$  and  $y$  directions, respectively. Substituting Eqs. (6)–(9) into Eq. (11), neglecting terms involving products of perturbation quantities, and canceling common exponential factors, we arrive at the linearized continuity equation

$$\frac{\partial}{\partial t} \delta \rho + \rho_1 \left( \frac{\partial}{\partial x} \delta u_x + ik \delta u_y \right) = 0. \quad (14)$$

Similarly, the  $x$  and  $y$  components of the momentum equation reduce to

$$\frac{\partial}{\partial t} \delta u_x + \frac{\partial}{\partial x} \frac{\delta p}{\rho_1} = 0, \quad (15)$$

$$\frac{\partial}{\partial t} \delta u_y + ik \frac{\delta p}{\rho_1} = 0. \quad (16)$$

In deriving Eq. (14), we have used the linearized form of Eq. (13), i.e.,  $d(\delta s)/dt = 0$ , and the thermodynamic relation  $\delta p = \delta p/c^2 + (\partial \rho / \partial s)_p \delta s$ . The partial derivative with respect to time of this latter equation allows us to write

$$\frac{\partial}{\partial t} \delta p - c^2 \frac{\partial}{\partial t} \delta \rho = 0. \quad (17)$$

Equations (14)–(17) constitute the linearized system of perturbed fluid equations governing the dynamics of a rippled, two-dimensional shock wave. Before they can be solved, though, these equations must be supplemented by boundary conditions, which we now discuss.

The boundary conditions for this problem are derived by applying the principles of mass and momentum conservation across the shock front. To apply these principles, we first need to find expressions for the normal and tangential unit vectors on the surface of the rippled shock (see Fig. 3). In the

approximation that is linear in the perturbation amplitudes, these unit vectors are given by

$$\hat{\mathbf{N}} = \hat{\mathbf{x}} - ik \delta x e^{iky} \hat{\mathbf{y}}, \quad (18)$$

$$\hat{\mathbf{T}} = ik \delta x e^{iky} \hat{\mathbf{x}} + \hat{\mathbf{y}}. \quad (19)$$

Note that in writing Eqs. (18) and (19), we have implicitly assumed that  $k \delta x \ll 1$ —a statement that gives precise meaning to the term “small” perturbation in the present context. With  $\mathbf{u}_s = \hat{\mathbf{x}} \partial x_s / \partial t$  denoting the perturbed shock velocity, conservation of mass requires that  $\rho(\mathbf{u}_s - \mathbf{u}) \cdot \hat{\mathbf{N}}$  be equal on both sides of the front. This leads to the first-order equation

$$\delta u_x = \frac{\eta - 1}{\eta} \frac{d}{dt} \delta x - \frac{D}{\eta} \frac{\delta \rho}{\rho_1}. \quad (20)$$

The zeroth-order contribution to the mass conservation equation is given by Eq. (3).

We now consider the implications of momentum conservation across the rippled shock. This principle states that the vector  $\rho(\mathbf{u}_s - \mathbf{u})(\mathbf{u}_s - \mathbf{u}) \cdot \hat{\mathbf{N}} + p \hat{\mathbf{N}}$  is the same on both sides of the front, which to zeroth order yields Eq. (4). Using the relation

$$\delta p = \left( \frac{dp}{d\rho} \right)_H \delta \rho = - \frac{D^2}{\eta^2 h} \delta \rho, \quad (21)$$

one can show after performing some algebra that the  $x$  component of the first-order momentum-conservation equation can be written as

$$\delta u_x = \frac{\eta}{2D} (h - 1) \frac{\delta p}{\rho_1}. \quad (22)$$

It should be noted that the relation between the first-order pressure and density amplitudes in Eq. (21) holds immediately behind the shock front only, and is merely a consequence of expanding the Hugoniot equation in a first-order Taylor series. Equation (22) can be combined with Eq. (20) to yield

$$\delta u_x = \frac{\eta - 1}{\eta} \left( \frac{1 - h}{1 + h} \right) \frac{d}{dt} \delta x, \quad (23)$$

$$\delta p = - \frac{2D\rho_1}{1+h} \left( \frac{\eta - 1}{\eta^2} \right) \frac{d}{dt} \delta x. \quad (24)$$

To complete our set of boundary conditions, we also need an expression for the transverse amplitude  $\delta u_y$ . This is obtained by enforcing continuity of the transverse component of velocity across the shock front. The result is

$$\delta u_y = ikD \frac{\eta - 1}{\eta} \delta x. \quad (25)$$

The presence of the factor  $i$  in Eq. (25) implies that the transverse velocity perturbation is  $90^\circ$  out of phase with the ripple on the surface of the shock.

In order to simplify the statement of our problem, it is useful at this stage to introduce the normalized space and time variables  $\xi = kx$  and  $\tau = D k t / \eta$ , along with the following definitions:

$$g(\tau) \equiv k \left( \frac{\eta - 1}{\eta} \right) \delta x, \quad (26)$$

$$\phi(\xi, \tau) \equiv \frac{\eta^2}{D^2} \frac{\delta p}{\rho_1}, \quad (27)$$

$$\psi_x(\xi, \tau) \equiv \frac{\eta}{D} \delta u_x, \quad (28)$$

$$\psi_y(\xi, \tau) \equiv \frac{\eta}{D} \delta u_y. \quad (29)$$

Employing Eqs. (26)–(29), the linearized mass and momentum equations [Eqs. (14)–(16)] can be cast in dimensionless form as

$$i \psi_y + \frac{\partial \psi_x}{\partial \xi} + M_1^2 \frac{\partial \phi}{\partial \tau} = 0, \quad (30)$$

$$\frac{\partial \psi_x}{\partial \tau} + \frac{\partial \phi}{\partial \xi} = 0, \quad (31)$$

$$\frac{\partial \psi_y}{\partial \tau} + i \phi = 0, \quad (32)$$

where we have used Eq. (17) to eliminate  $\delta \rho$  from Eq. (14). These equations are subject to the boundary conditions

$$\psi_x(-\tau, \tau) = \frac{1-h}{1+h} g'(\tau), \quad (33)$$

$$\psi_y(-\tau, \tau) = i \eta g(\tau), \quad (34)$$

$$\phi(-\tau, \tau) = -\frac{2}{1+h} g'(\tau), \quad (35)$$

at the shock front, whose position in normalized variables is given by  $\xi = -\tau$ . Note that in Eqs. (33) and (35), the prime on  $g(\tau)$  denotes differentiation with respect to the variable  $\tau$ .

The system of first-order, partial-differential equation appearing in Eqs. (30)–(32) can be reduced to a single second-order equation for the dimensionless pressure amplitude  $\phi$  by taking the  $\tau$  derivative of Eq. (30), subtracting from it the  $\xi$  derivative of Eq. (31), and employing Eq. (32). Following this procedure, we find

$$-\frac{\partial^2 \phi}{\partial \xi^2} + M_1^2 \frac{\partial^2 \phi}{\partial \tau^2} + \phi = 0, \quad (36)$$

which is a homogeneous, two-dimensional wave equation that has been Fourier transformed in one spatial variable. In passing, we note that Eq. (36) is equivalent to the Klein-Gordon equation for describing the dynamics of a “scalar”

meson in quantum mechanics [37]. An equation with the same form as Eq. (36) also governs the behavior of a flexible string with additional stiffness forces provided by its surrounding medium (e.g., a string embedded in a sheet or rubber) [38]. This equation is subject to Cauchy-type (Dirichlet and Neumann) conditions at the initial instant, and at the surface of the shock. Since Eq. (36) is hyperbolic, this a well-posed problem possessing a unique, stable solution [39]. The initial conditions that  $\phi$  must obey are

$$\phi(\xi, 0) \equiv \phi_0(\xi), \quad (37)$$

$$\frac{\partial \phi}{\partial \tau}(\xi, 0) = -M_1^{-2} \left[ i \psi_y(\xi, 0) + \frac{\partial \psi_x}{\partial \xi}(\xi, 0) \right], \quad (38)$$

where the latter expression results from Eq. (30). At the shock front,  $\phi$  must satisfy Eq. (35) at all times, as well as a Neumann-type boundary condition, which can be derived by subtracting Eq. (30) from Eq. (31), and using the total  $\tau$  derivative of Eq. (33), where

$$\frac{d}{d\tau} = \frac{\partial}{\partial \tau} - \frac{\partial}{\partial \xi} \quad \text{when} \quad \xi = -\tau.$$

The result is

$$\frac{1-h}{1+h} g''(\tau) + \eta g(\tau) = - \left( \frac{\partial \phi}{\partial \xi} - M_1^2 \frac{\partial \phi}{\partial \tau} \right)_{\xi=-\tau}. \quad (39)$$

The remainder of this paper is devoted to finding an explicit solution to Eq. (36), subject to the conditions specified in Eqs. (33)–(35) and Eqs. (37)–(39). We should point out, though, that the result of our analysis does not yield the normalized pressure amplitude  $\phi$  directly; instead we choose to solve for the time-dependent ripple amplitude  $g(\tau)$ , since that quantity is more easily compared with results from numerical simulations. Once  $g(\tau)$  is determined, the function  $\phi$  can in principle be found by recourse to the governing system of equations (although that step is not performed in the present study).

It is somewhat instructive to compare Eq. (39) with the equation governing damped harmonic motion [40]:

$$m r''(t) + \kappa r(t) = -\nu r'(t). \quad (40)$$

Here, the quantities  $m$ ,  $\kappa$ , and  $\nu$  are constants, and the function  $r(t)$  represents some time-dependent amplitude (e.g., the position of a mass connected to a spring on a frictional surface). From this comparison, we see that Eq. (39) may be viewed as a harmonic oscillator equation with a complicated damping term—i.e., one that is not simply proportional to the velocity of motion. As we shall see, the evolution of the ripple amplitude  $g(\tau)$  in Eq. (39) does superficially resemble the attenuated “ringing” of a damped harmonic oscillator, but with the important distinctions that the frequency of oscillation is not constant, and that the damping factor is not simply an exponential function of time.

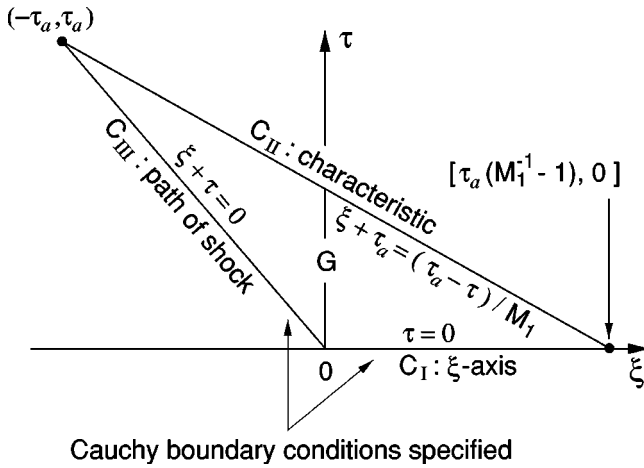


FIG. 4. Space-time diagram of shock and sound wave that define the solution region  $G$  at the time  $\tau_a$ . This region is bounded by the contour  $C$ , which comprises three line segments:  $C_I$ ,  $C_{II}$ , and  $C_{III}$ . The first extends along the  $\xi$  axis from 0 to  $\tau_a(M_1^{-1}-1)$ , the second lies on the characteristic  $\xi + \tau_a = (\tau_a - \tau)/M_1$ , and the third coincides with the path of the shock wave given by  $\xi + \tau = 0$ .

### III. AN INTEGRAL EXPRESSION FOR THE RIPPLE AMPLITUDE

In this section, we outline our strategy for solving Eq. (36), which is a linear, hyperbolic, partial-differential equation. Following Roberts [3], we begin our analysis by noting that this equation possesses the characteristics

$$\xi - \xi_a = \pm (\tau_a - \tau)/M_1. \quad (41)$$

Here,  $\xi_a$  and  $\tau_a$  are constants, and refer to an arbitrary point in the plane define by the variables  $\xi$  and  $\tau$ . If we choose this point to correspond to the position of the shock at the time  $\tau_a$  so that  $\xi_a = -\tau_a$ , we see that only one of the characteristics comes from the shocked material—namely, the one preceded by a “+” sign in Eq. (41). Thus, we conclude that conditions at the front are influenced only by what occurs in the region  $G$  defined by

$$\tau \geq 0,$$

$$\xi + \tau \geq 0,$$

$$\xi + \tau_a \leq (\tau_a - \tau)/M_1.$$

This region is bounded by the contour  $C$ , which comprises three line segments, as shown in Fig. 4. The first extends along the  $\xi$  axis from 0 to  $\tau_a(M_1^{-1}-1)$ , the second along the characteristic  $\xi + \tau_a = (\tau_a - \tau)/M_1$ , and the third along the shock-wave path  $\xi + \tau = 0$ . For convenience, we shall refer to these three line segments as  $C_I$ ,  $C_{II}$ , and  $C_{III}$ , respectively. Note that in the dimensionless units of this problem, the speed of sound is given by  $1/M_1$ .

We now seek a solution to Eq. (36) within the region  $G$ . Since Cauchy boundary conditions are to be imposed on only two of the three bounding line segments—i.e., along  $C_I$  and  $C_{III}$ , but not along the characteristic  $C_{II}$ —this region is

classified as an “open surface,” and so we may expect to find a unique and stable solution there [39]. We proceed by employing a method due to Riemann for solving hyperbolic partial-differential equations (analogous to the theory of Green functions for elliptic operators) [38]. This method relies on choosing an appropriate “Riemann function”  $f(\xi, \tau | \xi', \tau')$ , which in our case should be a particular solution of Eq. (36). The function  $f$  must also obey the reciprocity relation  $f(\xi, \tau | \xi', \tau') = f(\xi', \tau' | \xi, \tau)$ . Here, the primed coordinates refer to an arbitrary point in the space-time diagram of Fig. 4. Such a function can be easily found by assuming that it depends only on the quantity

$$R = \sqrt{(\tau' - \tau)^2/M_1^2 - (\xi' - \xi)^2}.$$

Substitution of  $f(R)$  into Eq. (36) leads to a Bessel equation, with the solution

$$f(R) = J_0(\sqrt{(\tau' - \tau)^2/M_1^2 - (\xi' - \xi)^2}).$$

The symbol  $J_0$  in this expression denotes a Bessel function of order zero. Note that the Neumann function, which is the second solution of Bessel’s equation, is disqualified for use in the present context since it is singular at  $R=0$ . For the primed coordinates in  $f(R)$ , we choose  $\xi' = -\tau_a$  and  $\tau' = \tau_a$ .

Let us demonstrate how the Riemann function  $f(R)$  can be used to reduce Eq. (36) to an integral equation for the ripple amplitude  $g(\tau)$ . The first step is to define the operator

$$\mathcal{G} = -\frac{\partial^2}{\partial \xi^2} + M_1^2 \frac{\partial^2}{\partial \tau^2}$$

and introduce the vector

$$\mathbf{V} = \left( \phi \frac{\partial f}{\partial \xi} - f \frac{\partial \phi}{\partial \xi} \right) \hat{\xi} + M_1^2 \left( f \frac{\partial \phi}{\partial \tau} - \phi \frac{\partial f}{\partial \tau} \right) \hat{\tau},$$

where  $\hat{\xi}$  and  $\hat{\tau}$  are unit vectors in the  $\xi$  and  $\tau$  directions, respectively. An important property of  $\mathbf{V}$  is that it is solenoidal:  $\nabla \cdot \mathbf{V} = f \mathcal{G} \phi - \phi \mathcal{G} f = 0$ . Next, we compute the line integral of this vector around the contour  $C$  by employing the two-dimensional form of Gauss’ theorem:

$$\int_G \nabla \cdot \mathbf{V} d^2x = \oint_C \mathbf{V} \cdot \hat{n} d\ell, \quad (42)$$

where  $\hat{n}$  is an outward-pointing unit vector and  $d\ell$  is an infinitesimal line segment. Then, using Eq. (42), and the expressions for  $\hat{n} d\ell$  along  $C_I$ ,  $C_{II}$ ,  $C_{III}$  listed in Table I, we find

TABLE I. Quantities along the line segments  $C_I$ ,  $C_{II}$ , and  $C_{III}$ , which comprise the contour  $C$  in Eq. (42). The parameter  $\alpha$  is defined in Eq. (44).

	$C_I$	$C_{II}$	$C_{III}$
$\hat{n} d\ell$	$-\hat{\tau} d\xi$	$\hat{\xi} d\tau + \hat{\tau} d\tau/M_1$	$-(\hat{\xi} + \hat{\tau})d\tau$
$f$	$J_0(\sqrt{\tau_a^2/M_1^2 - (\xi + \tau_a)^2})$	1	$J_0(\alpha(\tau_a - \tau))$
$\frac{\partial f}{\partial \tau}$	$\frac{\tau_a J_1(\sqrt{\tau_a^2/M_1^2 - (\xi + \tau_a)^2})}{M_1^2 \sqrt{\tau_a^2/M_1^2 - (\xi + \tau_a)^2}}$	$\frac{(\tau_a - \tau)}{2M_1^2}$	$\frac{J_1(\alpha(\tau_a - \tau))}{\alpha M_1^2}$
$\frac{\partial f}{\partial \xi}$	$\frac{(\xi + \tau_a) M_1^2}{\tau_a} \frac{\partial f}{\partial \tau}$	$M_1 \frac{\partial f}{\partial \tau}$	$M_1^2 \frac{\partial f}{\partial \tau}$

$$0 = -M_1^2 \int_0^{(1-M_1)\tau_a/M_1} \left( f \frac{\partial \phi}{\partial \tau} - \phi \frac{\partial f}{\partial \tau} \right)_{C_I} d\xi + \int_0^{\tau_a} \left[ M_1 \left( f \frac{\partial \phi}{\partial \tau} - \phi \frac{\partial f}{\partial \tau} \right) - \left( f \frac{\partial \phi}{\partial \xi} - \phi \frac{\partial f}{\partial \xi} \right) \right]_{C_{II}} d\tau - \int_0^{\tau_a} \left[ M_1^2 \left( f \frac{\partial \phi}{\partial \tau} - \phi \frac{\partial f}{\partial \tau} \right) - \left( f \frac{\partial \phi}{\partial \xi} - \phi \frac{\partial f}{\partial \xi} \right) \right]_{C_{III}} d\tau.$$

Values for  $f$ ,  $\partial f/\partial \tau$ , and  $\partial f/\partial \xi$  are also given in Table I. Substituting these expressions into the equation above, making use of Eq. (35) and Eqs. (37)–(39), and noting that

$$\frac{d}{d\tau} = \frac{\partial}{\partial \tau} - \frac{1}{M_1} \frac{\partial}{\partial \xi} \quad \text{when} \quad \xi + \tau_a = (\tau_a - \tau)/M_1$$

leads to

$$\frac{2M_1}{1+h} g'(\tau_a) + \int_0^{\tau_a} \left[ \frac{1-h}{1+h} g''(\tau) + \eta g(\tau) \right] J_0(\alpha(\tau_a - \tau)) d\tau = \chi(\tau_a), \quad (43)$$

where

$$\alpha \equiv \sqrt{\frac{1-M_1^2}{M_1^2}} \quad (44)$$

and

$$\chi(\tau_a) = -M_1 \phi_0 \left( \frac{1-M_1}{M_1} \tau_a \right) + \int_0^{(1-M_1)\tau_a/M_1} d\xi \left\{ \left[ i\psi_y(\xi,0) + \frac{\partial \psi_x}{\partial \xi}(\xi,0) \right] \times J_0(\sqrt{(\tau_a/M_1)^2 - (\xi + \tau_a)^2}) + \frac{J_1(\sqrt{(\tau_a/M_1)^2 - (\xi + \tau_a)^2})}{\sqrt{(\tau_a/M_1)^2 - (\xi + \tau_a)^2}} \tau_a \phi_0(\xi) \right\}. \quad (45)$$

In certain limiting cases, the complexity of this last equation can be reduced considerably. For example, if we consider an initial perturbation consisting of a sinusoidal deformation to a planar shock front (with unperturbed hydrodynamic quantities behind it) we have

$$\chi(\tau_a) = \frac{h-1}{h+1} g'(0) J_0(\alpha \tau_a), \quad (46)$$

which is valid for  $\tau_a > 0$ . This equation results from setting the quantities  $\phi_0(\xi)$ ,  $\psi_x(\xi,0)$ , and  $\psi_y(\xi,0)$ —but not  $\partial \psi_x(\xi,0)/\partial \xi$ —equal to zero for  $\xi > 0$  in Eq. (45). Note that for this initial condition, the function  $\chi$  is discontinuous at  $\tau_a = 0$ , where it assumes the value  $2M_1 g'(0)/(1+h)$ .

In order to cast Eq. (43) in a more useful form, we manipulate it according to the following procedure. First, we change the variable of integration from  $\tau$  to  $\theta$ . Next, we substitute the variable  $\tau$  for  $\tau_a$ . Finally, we perform an integration by parts, and then integrate the entire resulting expression with respect to  $\tau$ . The result of all these operations is a Volterra equation of the second kind [41] for the ripple amplitude:

$$g(\tau) = F(\tau) + \int_0^\tau g(\theta) K(\tau - \theta) d\theta, \quad (47)$$

where the kernel  $K(q)$  is given by

$$K(q) = \frac{\alpha(1-h)}{1+2M_1-h} \left[ J_1(\alpha q) - \frac{\eta(1+h)}{\alpha^2(1-h)} \int_0^{\alpha q} J_0(w) dw \right] \quad (48)$$

and the function  $F(\tau)$  is

$$F(\tau) = g(0) + \frac{1+h}{1+2M_1-h} \times \left\{ \int_0^\tau \left[ \chi(w) - \frac{h-1}{h+1} g'(0) J_0(\alpha w) \right] dw + \frac{h-1}{h+1} g(0) [1 - J_0(\alpha \tau)] \right\}. \quad (49)$$

For the case of a planar shock front initially deformed into a sinusoidal shape, we have

$$F(\tau) = \frac{g(0)}{1+2M_1-h} [2M_1 + (1-h)J_0(\alpha \tau)]. \quad (50)$$

Note that  $F(0) = g(0)$ . In the following section, we show how the integral equation in Eq. (47) may be solved in this special case using the method of Laplace transforms.

#### IV. THE SOLUTION

The difficulty associated with an integral expression like the Volterra equation in Eq. (47) is, of course, the appearance both inside and outside of an integral sign of the unknown function that we seek [in our case the ripple amplitude  $g(\tau)$ ]. This fact greatly complicates a straightforward attempt at finding a solution. In such situations, one must often resort to indirect mathematical approaches such as integral

transform methods that map the sought-after function from one space (in our case  $\tau$ ) to another in which a solution is readily determined. Often, the challenge then lies in the inversion of the mapping procedure to express the final answer in terms of the original variable.

One such approach—the method of Laplace transforms [41]—is particularly well suited to the present class of problems. A fundamental axiom of this method is the convolution theorem [see Eq. (A9) in the Appendix], which permits us to convert Eq. (47) from an integral equation for  $g(\tau)$  into an algebraic one for  $g_L(s)$  — our shorthand notation for the Laplace transform of  $g(\tau)$ . Throughout our discussion, we shall use the subscript  $L$  to denote the Laplace transform of a function, where  $s$  is the associated transform variable (not to be confused with the specific entropy introduced in Sec. II); see the Appendix. Applying the convolution theorem to Eq. (47) and solving the resulting expression for  $g_L(s)$ , we find

$$g_L(s) = F_L(s) / [1 - K_L(s)].$$

Limiting our attention to the special initial condition of a planar shock front deformed by a sinusoidal ripple, explicit expressions for  $F_L$  and  $K_L$  can be easily derived using Eqs. (A2)–(A5) in the Appendix. The result is that the transform of the ripple amplitude can be written as

$$\frac{g_L(s)}{g(0)} = \frac{\sqrt{s^2 + \alpha^2} + \beta s}{s \sqrt{s^2 + \alpha^2} + \beta s^2 + \Gamma}, \quad (51)$$

where we have introduced the definitions

$$\beta \equiv \frac{1-h}{2M_1}, \quad (52)$$

$$\Gamma \equiv \frac{(1+h)\eta}{2M_1}. \quad (53)$$

Our principal task in this section is to invert Eq. (51), and thus determine the time-dependent ripple amplitude  $g(\tau) = \mathcal{L}^{-1}\{g_L(s)\}$ , where the symbol  $\mathcal{L}^{-1}$  denotes the inverse Laplace-transform operator. Since this equation involves the quotient of irrational functions, though, such an inversion is not a trivial exercise, and requires special consideration.

The first step to finding the inverse Laplace transform of  $g_L(s)/g(0)$  is to rationalize the denominator in Eq. (51), which yields

$$\frac{g_L(s)}{g(0)} = \frac{(\beta^2 - 1)s^3 + (\beta\Gamma - \alpha^2)s + \Gamma\sqrt{s^2 + \alpha^2}}{(\beta^2 - 1)s^4 + (2\beta\Gamma - \alpha^2)s^2 + \Gamma^2}. \quad (54)$$

To proceed, we must now adopt a particular solution methodology. One obvious approach is to seek a solution of Eq. (54) by analyzing its poles and then computing the appropriate Bromwich integral using well-established methods from analytic function theory [39]. This procedure is somewhat involved, however, owing to the square root term in Eq. (54), which necessitates consideration of a branch cut in the complex plane. A slightly more-attractive possibility for inverting Eq. (54) is to factor it into a series of paired multiplicative

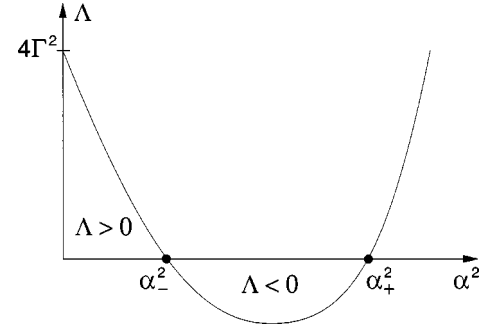


FIG. 5. Plot of  $\Lambda$  as a function of  $\alpha^2$ . The roots of  $\Lambda=0$  are denoted by  $\alpha_-^2$  and  $\alpha_+^2$ , as indicated in the figure. If  $\Lambda < 0$ , the value of  $\alpha^2$  lies between these two limits. For physical equations of state with  $\Lambda > 0$ , the value of  $\alpha^2$  is apparently restricted to be less than  $\alpha_-^2$ .

expressions (partial fractions), each of which can be recognized as a Laplace transform of a known function; the products of terms in this series can then be inverted through use of the convolution theorem. In this paper, we choose to pursue the latter strategy. In so doing, we must make sure that the result has no imaginary component, since  $g(\tau)$  is strictly a real quantity. This consideration leads to two ways of factoring Eq. (54), which in turn yields two families of solutions.

For reasons that will become clear shortly, the factoring method appropriate for a given ripple-shock system is determined by the sign of the quantity

$$\Lambda \equiv \alpha^4 - 4\beta\Gamma\alpha^2 + 4\Gamma^2. \quad (55)$$

Plotted as a function of  $\alpha^2$ , this expression forms a parabola, as shown in Fig. 5. The roots of  $\Lambda=0$  are easily shown to be

$$\alpha_{\pm}^2 = 2\Gamma(\beta \pm \sqrt{\beta^2 - 1}).$$

Note that the inequality  $\Lambda < 0$  is consistent with the value of  $\alpha^2$  lying between  $\alpha_-^2$  and  $\alpha_+^2$ . The condition  $\Lambda > 0$ , on the other hand, implies that  $\alpha^2 < \alpha_-^2$  or  $\alpha_+^2 < \alpha^2$ , but apparently only the former inequality is physical. In the derivation that follows, we shall assume that  $\alpha^2$  never exceeds  $\alpha_-^2$  when  $\Lambda > 0$ . Additionally, we require that  $\beta > 1$  and  $\Gamma > 0$  always—conditions that appear to be satisfied for most well-behaved equations of state. Let us now discuss the derivation of the solution for each sign of  $\Lambda$  separately.

#### A. The case $\Lambda > 0$

If the sign of  $\Lambda$  is positive, the denominator in Eq. (54) can be written as  $(\beta^2 - 1)$  times the product  $[s^2 + (a+b)^2] \times [s^2 + (a-b)^2]$ , where

$$(a \pm b)^2 = \frac{1}{2(\beta^2 - 1)} [2\beta\Gamma - \alpha^2 \pm \sqrt{\alpha^4 - 4\beta\Gamma\alpha^2 + 4\Gamma^2}], \quad (56)$$

and  $a$  and  $b$  are real constants given by

$$a = \sqrt{\frac{2\beta\Gamma - \alpha^2}{4(\beta^2 - 1)} + \frac{\Gamma}{2(\beta^2 - 1)^{1/2}}},$$

$$b = \sqrt{\frac{2\beta\Gamma - \alpha^2}{4(\beta^2 - 1)} - \frac{\Gamma}{2(\beta^2 - 1)^{1/2}}}.$$

Since  $\Lambda > 0$ , the right-hand side of Eq. (56) is a real quantity whose sign is positive by virtue of the inequality  $\alpha^2 < \alpha_-^2$ . Equation (54) can then be factored as

$$\frac{g_L(s)}{g(0)} = \frac{1}{s^2 + (a+b)^2} \left[ \frac{c_1}{s + \sqrt{s^2 + \alpha^2}} + c_2 s \right] + \frac{1}{s^2 + (a-b)^2} \left[ \frac{c_3}{s + \sqrt{s^2 + \alpha^2}} + c_4 s \right], \quad (57)$$

where the (real) constants  $c_1, c_2, c_3,$  and  $c_4$  are given by

$$c_1 = \frac{-\alpha^2\Gamma}{\sqrt{\alpha^4 - 4\beta\Gamma\alpha^2 + 4\Gamma^2}} = -c_3,$$

$$c_2 = \frac{1}{2} - \frac{\Gamma - \alpha^2/2}{\sqrt{\alpha^4 - 4\beta\Gamma\alpha^2 + 4\Gamma^2}} = 1 - c_4.$$

Consulting Eqs. (A6)–(A8) in the Appendix, we see that Eq. (57) is in the form of products of transforms involving trigonometric and Bessel functions. Using the convolution theorem [Eq. (A9)], this expression can be inverted to give

$$\begin{aligned} \frac{g(\tau)}{g(0)} &= \frac{c_1}{a+b} \int_0^\tau \sin[(a+b)(\tau-z)] \frac{J_1(\alpha z)}{\alpha z} dz \\ &+ c_2 \cos(a+b)\tau + \frac{c_3}{a-b} \int_0^\tau \sin[(a-b)(\tau-z)] \\ &\times \frac{J_1(\alpha z)}{\alpha z} dz + c_4 \cos(a-b)\tau, \end{aligned}$$

where the symbol  $J_1$  denotes a Bessel function of order one. In the case that  $a \pm b > \alpha$  (which holds for all ideal gases) one can show using Eq. (A10) that all purely oscillatory terms in the above expression cancel. If  $a+b$  and/or  $a-b$  are/is less than  $\alpha$ , some oscillatory terms persist and *stationary* perturbations—which neither grow nor attenuate in time—result. We shall not discuss this unusual phenomenon further here, but simply remark that it is likely associated with the D’yakov-Kontorovich instability of shock waves [5,42–45].

Assuming  $a \pm b > \alpha$ , the solution for  $\Lambda > 0$  can be written after some manipulation as

$$\begin{aligned} \frac{g(\tau)}{g(0)} &= \frac{2\alpha^2\sqrt{\beta^2-1}}{\sqrt{\alpha^4-4\beta\Gamma\alpha^2+4\Gamma^2}} \\ &\times \int_0^\infty (b \sin az \cos bz - a \cos az \sin bz) \\ &\times \frac{J_1(\alpha(\tau+z))}{\alpha(\tau+z)} dz, \end{aligned} \quad (58)$$

where the relation  $\int_0^\tau \dots dz = \int_0^\infty \dots dz - \int_\tau^\infty \dots dz$  has been used. Employing Eq. (A10) in the Appendix, one can show that the right-hand side of Eq. (58) has the correct normalization (i.e., assumes the value unity) for  $\tau=0$ . Furthermore, from the asymptotic form of the first-order Bessel function,  $J_1(q) \sim \sqrt{2/(\pi q)} \cos[q-3/(4\pi)]$  for  $q \rightarrow \infty$ , we see that the amplitude  $g(\tau)$  undergoes oscillations that die out as  $\tau^{-3/2}$  late in time. This asymptotic dependence, which has been observed previously in both shock-tube [16,46] and laser-driven ICF [12] experiments, is apparently a general property of perturbed shock fronts that extends beyond the isolated variety considered in this paper [13].

### B. The case $\Lambda < 0$

If the discriminant  $\Lambda$  is negative, Eq. (54) must be factored differently to yield a real expression for  $g(\tau)/g(0)$ . In this case, we find that Eq. (57) should be written as

$$\begin{aligned} \frac{g_L(s)}{g(0)} &= \frac{1}{(s+\sigma)^2 + a^2} \left[ \frac{d_1 + d_2 s}{s + \sqrt{s^2 + \alpha^2}} + d_3 s + d_4 \right] \\ &+ \frac{1}{(s-\sigma)^2 + a^2} \left[ \frac{d_5 + d_6 s}{s + \sqrt{s^2 + \alpha^2}} + d_7 s + d_8 \right], \end{aligned} \quad (59)$$

where the quantity  $\sigma = -ib$  is real and positive. The constants  $d_1, d_2, d_3,$  and  $d_4$  in Eq. (59) are given by

$$\begin{aligned} d_1 &= \frac{\alpha^2}{2\sqrt{\beta^2-1}} = d_5, \\ d_2 &= \frac{\alpha^2}{2\sqrt{\alpha^2-2\beta\Gamma+2\Gamma(\beta^2-1)^{1/2}}} = -d_6, \end{aligned}$$

$$d_3 = \frac{1}{2} = d_7,$$

$$d_4 = \frac{\Gamma + [\alpha^2 - (1 + \beta)\Gamma](\beta^2 - 1)^{-1/2}}{2\sqrt{\alpha^2 - 2\beta\Gamma + 2\Gamma(\beta^2 - 1)^{1/2}}} = -d_8.$$

Once again, Eq. (59) has the form of products of transformed functions that can be easily recognized. Using the convolution theorem and Eqs. (A6)–(A8) in the Appendix, we find that the solution for  $\Lambda < 0$  is

$$\begin{aligned}
\frac{g(\tau)}{g(0)} = & \frac{1}{2} e^{-\sigma\tau} \cos a\tau - \left[ \frac{\Gamma}{\beta^2 - 1} - \frac{\alpha^2}{2(\beta^2 - 1)} \right] \frac{e^{-\sigma\tau} \sin a\tau}{4a\sigma} \\
& + \frac{\alpha^2}{4\sigma\sqrt{\beta^2 - 1}} \left\{ \int_0^\tau e^{-\sigma(\tau-z)} \left[ \cos a(\tau-z) \right. \right. \\
& + \frac{\sigma}{a} \sin a(\tau-z) \left. \left. \right] \frac{J_1(\alpha z)}{\alpha z} dz \right. \\
& \left. + \int_0^\infty e^{-\sigma z} \left[ \cos az + \frac{\sigma}{a} \sin az \right] \frac{J_1(\alpha(\tau+z))}{\alpha(\tau+z)} dz \right\}. \tag{60}
\end{aligned}$$

In arriving at this expression, we have made use of Eqs. (A11) and (A12) to cancel all nonevanescing terms. The presence of decaying exponential functions in Eq. (60) tends to enhance the initial damping of shock-ripple oscillations, and thereby serves to distinguish this family of solutions from that in Eq. (58). Note, though, that for both families the asymptotic dependence as  $\tau \rightarrow \infty$  is the same, namely,  $\tau^{-3/2}$  times an oscillatory function of  $\tau$ .

The same asymptotic behavior holds if the discriminant  $\Lambda$  vanishes—an event that can occur at isolated points along the Hugoniot curve for realistic equations of state. In this case, the roots  $(a \pm b)^2$  in Eq. (56) are identical and the factoring of  $g_L(s)/g(0)$  is somewhat different than in Eq. (57) or (59). We shall not provide the details of the calculation for  $\Lambda=0$ , but simply quote the final result, which is

$$\begin{aligned}
\frac{g(\tau)}{g(0)} = & \sqrt{a^2 - \alpha^2} \\
& \times \int_0^\infty (\sin az - az \cos az) \frac{J_1(\alpha(\tau+z))}{\alpha(\tau+z)} dz, \tag{61}
\end{aligned}$$

where  $\alpha = \alpha_-$ . It should be emphasized here that the ripple amplitude  $g(\tau)$  undergoes a *continuous* transition from one family of solutions to the other as  $\Lambda$  changes sign. That is, in the limit that  $\Lambda \rightarrow 0$ , both Eqs. (58) and (60) smoothly approach the solution appearing in Eq. (61).

We should also remark that although Eqs. (58) and (60) were obtained by analyzing a *single* Fourier mode of the shock-front perturbation, the same solutions apply to all normalized amplitudes in a linearized multimode description. Since  $g(\tau)$  and  $g(0)$  are both proportional to  $k$ , the wave number enters the normalized solution  $g(\tau)/g(0)$  only through the independent variable  $\tau = Dkt/\eta$ . As a result, we see that shorter-wavelength perturbations die out earlier than longer ones. This property has been verified through numerical simulations of the type described in the following section, although we shall not present evidence of it in our discussion. Instead, we limit our attention to the consideration of single-mode perturbations only. This is done in an effort to underscore the differences in the attenuation properties of the two families of solutions, as well as facilitate comparison with our numerical results.

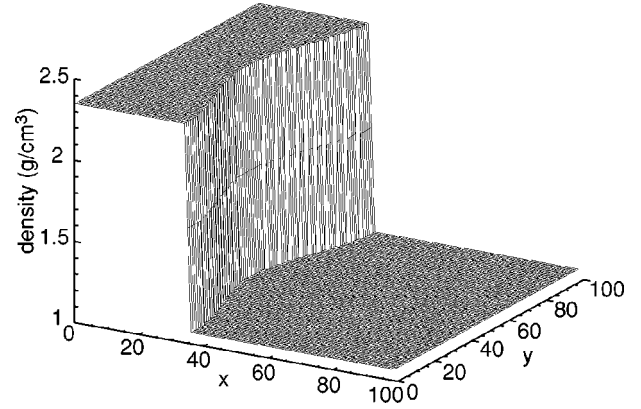


FIG. 6. An example of a perturbed density surface at the start of a FAST2D simulation. The ratio of ripple amplitude to wavelength in this study is 5%. Periodic boundaries are assumed in the transverse direction, and inflow and outflow conditions are imposed at the left and right ends, respectively, of the computational domain.

## V. COMPARISONS WITH NUMERICAL RESULTS

In this section, we wish to test the validity of Eqs. (58) and (60) by comparing their predictions against results from two-dimensional computer simulations. Several examples are considered for this purpose that illustrate behavior from both families of solutions. The simulations were performed on a fixed, two-dimensional numerical grid using a Cartesian version of NRL's ICF code FAST2D [21], with the thermal conduction and radiation transport modules turned off. Used in this way, the FAST2D code solves the conservation equations of hydrodynamics in Eulerian form via a flux-corrected transport algorithm (FCT) [47]. All nonideal EOS data required for this study were derived from the CALEOS material database.

A typical initial condition for our simulations appears in Fig. 6, which shows a sinusoidal perturbation superimposed on a two-dimensional shock front moving into a quiescent homogeneous fluid medium on the right. The size of the computational grid was approximately  $700 \times 100$  cells, but in Fig. 6, only the first 100 cells in the  $x$  direction are shown. Also note that this figure shows only a perturbed density profile, but the pressure and  $x$  component of velocity surfaces (not shown) were initially deformed with the same sinusoidal ripple. The  $y$  component of velocity was left unperturbed and initially set to zero everywhere. (We should point out that our choice of initial conditions here implies that the Rankine-Hugoniot relations [29] were not strictly satisfied in the simulations at  $\tau = 0$ ; this unphysical situation was quickly remedied by the FCT hydroalgorithm after a few time steps, however, with no noticeable corruption of the numerical results.) The simulations were allowed to evolve from this initial state for a duration equal to at least one-and-a-half ripple-oscillation periods. The output from the simulations were then postprocessed to measure the evolution of the ripple amplitude as a function of time.

A schematic of the method used to determine the temporal

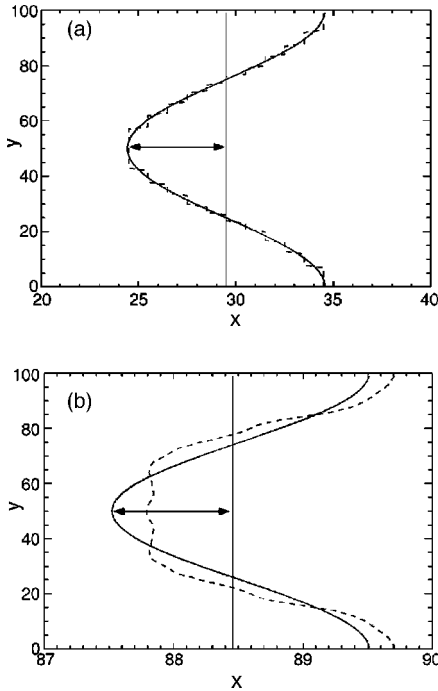


FIG. 7. Schematic of the method used for determining the shock-ripple amplitude in the FAST2D simulations (a) initially and (b) at a later time  $\tau > 0$ .

evolution of the shock-ripple amplitude appears in Fig. 7. The first task was to determine the position of the deformed shock front by computing a contour midway between the unperturbed upstream and downstream density states. Since the representation of a smoothly varying corrugation to the shock front on a two-dimensional Cartesian grid is only piecewise continuous—i.e., discontinuities exist between adjacent transverse grid cells—the initial contour in Fig. 7(a) has a “stair-step” appearance, and was Fourier transformed and filtered to extract the fundamental mode. The same filtering procedure was performed at every subsequent stage of the calculation, as shown in Fig. 7(b) for a time  $\tau > 0$ . The fundamental modes appear as solid curves in the figures, along with the positions of the unperturbed fronts (solid vertical lines). The evolution of the shock-ripple amplitude was then found by computing—at a fixed transverse location—the distance between these curves as a function of time. Once normalized by the initial shock-ripple amplitude, this distance (indicated by a double-headed arrow in each subfigure) gives an estimate for  $g(\tau)/g(0)$ , which can then be compared to theoretical predictions based on either Eq. (58) or (60).

Such a comparison is shown in Fig. 8 for four different rippled-shock systems. They are (a) a shock with  $M_0=3$  propagating through an ideal gas with  $\gamma=5/3$ , where  $\gamma$  is the ratio of specific heats; (b) a 1 Mbar shock in polystyrene; (c)

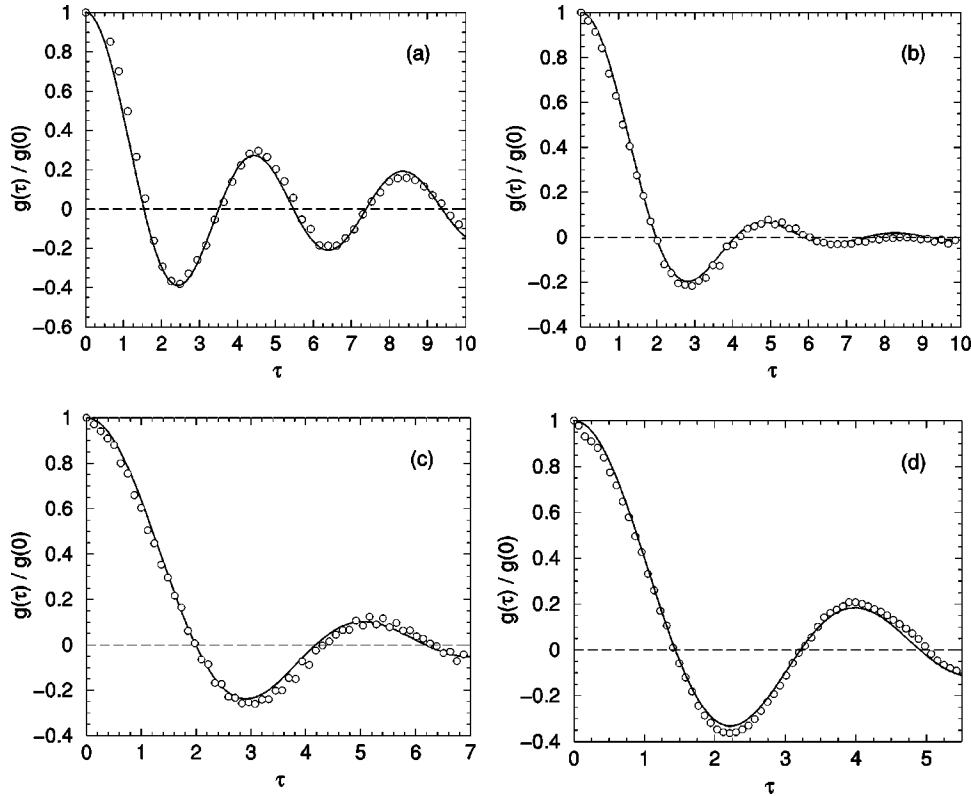


FIG. 8. Comparison of theoretical predictions (solid lines) and FAST2D simulation results (open circles) for the normalized ripple amplitude of a perturbed shock wave propagating through (a) an ideal gas, (b) polystyrene, (c) aluminum, and (d) deuterium-tritium ice. In (a), the ratio of specific heats is  $\gamma=5/3$  and the unperturbed Mach number is  $M_0=3$ . In (b), (c), and (d), the unperturbed shock strengths are 1, 5, and 0.5 Mbar, respectively. The example in (a) belongs to the family of solutions for which  $\Lambda > 0$ ; those in (b), (c), and (d) correspond to  $\Lambda < 0$ .

TABLE II. Parameters for the isolated rippled-shock examples considered in this paper. The labels CH, Al, and D-T stand for polystyrene, aluminum, and deuterium-tritium, respectively. The entries in the last three columns were computed using the CALEOS database.

	Ideal gas ( $\gamma=5/3, M_0=3$ )	CH (1 Mbar)	Al (5 Mbar)	D-T (0.5 Mbar)
$\rho_0$		1.07 g/cm <sup>3</sup>	2.71 g/cm <sup>3</sup>	0.25 g/cm <sup>3</sup>
$\rho_1$	$3 \rho_0$	2.350 g/cm <sup>3</sup>	6.257 g/cm <sup>3</sup>	0.7903 g/cm <sup>3</sup>
$T_0$		300 K	300 K	19 K
$T_1$	$11 T_0$	$5.290 \times 10^3$ K	$1.879 \times 10^4$ K	$8.969 \times 10^3$ K
$p_0$	<sup>a</sup>	$1.779 \times 10^{-2}$ Mbar	$1.813 \times 10^{-2}$ Mbar	$8.917 \times 10^{-4}$ Mbar
$p_1$	$11 p_0$	1 Mbar	5 Mbar	0.5 Mbar
$D$	$\sqrt{15 p_0/\rho_0}$	$1.298 \times 10^6$ cm/s	$1.801 \times 10^6$ cm/s	$1.709 \times 10^6$ cm/s
$c$	$\sqrt{55 p_0/(9 \rho_0)}$	$1.236 \times 10^6$ cm/s	$1.523 \times 10^6$ cm/s	$1.207 \times 10^6$ cm/s
$\eta$	3	2.197	2.309	3.161
$h$	-0.1111	-0.1647	-0.2071	$-8.448 \times 10^{-2}$
$M_0$	3	5.868	3.355	11.72
$M_1$	0.5222	0.4782	0.5120	0.4478
$\alpha_-^2$	3.577	2.006	1.983	3.413
$\alpha^2$	2.667	3.375	2.812	3.988
$\alpha_+^2$	7.289	7.343	6.449	12.24
$\beta$	1.064	1.218	1.179	1.211
$\Gamma$	2.553	1.919	1.788	3.232
$a$	2.961	1.433	1.527	2.103
$b$	1.316	0.8412 <i>i</i>	0.7303 <i>i</i>	0.5551 <i>i</i>
$(a-b)^2$	2.706	1.346-2.411 <i>i</i>	1.799-2.230 <i>i</i>	4.115-2.335 <i>i</i>
$(a+b)^2$	18.29	1.346+2.411 <i>i</i>	1.799+2.230 <i>i</i>	4.115+2.335 <i>i</i>
$\sigma$	-1.316 <i>i</i>	0.8412	0.7303	0.5551
$\Lambda$	4.214	-5.419	-3.015	-4.747

<sup>a</sup>Assuming  $\rho_0$  and  $T_0$  are independent, we have  $p_0 = \mathcal{R}\rho_0 T_0/m$ , where  $\mathcal{R} = 8.317 \times 10^7$  erg/deg mole is the universal gas constant and  $m$  is the molecular weight of the gas.

a 5 Mbar shock in aluminum; and (d) a 0.5 Mbar shock in a cryogenic mixture of deuterium and tritium. (The Mach numbers in the latter three cases were chosen so that the internal energy of the shocked material would exceed by many times the binding energy of the constituent atoms, thus warranting a hydrodynamic analysis, and justifying our use of the term “fluid medium” to describe material initially in a condensed state [29].) In Fig. 8, theoretical predictions are indicated by solid lines and simulation results are denoted by open circles. The relevant shock parameters for each system are listed in Table II. For the ideal-gas shock, we see that the value of  $\Lambda$  is positive, while the other three examples belong to the family of solutions for which  $\Lambda$  is negative. In all cases, the agreement between theoretical prediction and numerical simulation is quite good, which supports the validity of Eqs. (58) and (60). Note that for the examples shown in Fig. 8, the initial period of oscillation is the time required for the shock to travel a distance of about one to two perturbation wavelengths into the fluid ahead of it. This period does not remain constant, of course, but changes over time and asymptotically approaches the value  $2\pi\eta/(\alpha kD)$ —a result that applies to both families of solutions.

## VI. SUMMARY AND CONCLUSIONS

In this paper, we have generalized an earlier analysis by Roberts [3] to derive explicit expressions governing the tem-

poral evolution of perturbations to an isolated planar shock propagating through a material with an arbitrary EOS. It was shown that under most circumstances, at least two families of stable solutions exist. Membership in one family or the other for a particular shock-wave system is determined by the sign of the dimensionless quantity  $\Lambda$  [defined in Eq. (55)], which is a function of the strength of the shock, and the EOS properties of the material through which it propagates. For  $\Lambda > 0$ , one family of solutions applies [Eq. (58)], while for  $\Lambda < 0$ , a slightly different family [Eq. (60)] governs the evolution of the rippled shock wave. Both families of solutions share the same late-time behavior in that the envelope of oscillations falls off asymptotically as  $t^{-3/2}$ , but differ in the degree of damping that is present initially. In general, solutions for which  $\Lambda < 0$  are more strongly damped than those with  $\Lambda > 0$ .

It is interesting to note that the attenuated shock-front oscillations discussed in this paper qualitatively resemble the damped vibrations of a plucked string immersed in a viscous liquid [48]. In the latter case, the dynamics are governed by a differential equation similar to Eq. (40), where the frictional term  $-\nu r'(t)$  accounts for Newtonian drag forces in the surrounding liquid that oppose the string’s motion. Work done against these viscous forces by the string drains kinetic energy from the vibrating system and converts it into heat, resulting in oscillations that evanesce over time. (We assume

here that the “radiation resistance” of the string [49]—which determines the amount of energy converted into sound—is negligible by comparison; since strings are known to be inefficient radiators of acoustic energy [48], this approximation appears to be well justified.) As the temperature of the liquid is raised, the magnitude of the viscous term diminishes [50], which lessens the damping experienced by the string.

The analogy of a vibrating string in a viscous liquid provides some insight into the difference between the two families of rippled-shock solutions in Eqs. (58) and (60). Bearing in mind the conventional microscopic theory of liquids [51], this analogy suggests that the strongly damped shock-front oscillations for equations of state with  $\Lambda < 0$  are likely a reflection of appreciable forces of molecular interaction in the downstream medium, particularly at high densities and relatively low temperatures [29,52]. At higher temperatures, such “viscous” interactions become less significant, and the behavior resembles that of a perfect gas for which  $\Lambda > 0$ . These assertions are supported by the fact that one sees an eventual (and continuous) transition from the family of solutions with  $\Lambda < 0$  to that with  $\Lambda > 0$  for sufficiently strong shocks, as shown in Fig. 2(c) for the case of deuterium-tritium ice. Although not indicated in Fig. 2, it was noted during the course of this study that a similar sign change in  $\Lambda$  occurs for shocks in polystyrene and aluminum at approximately 23 and 50 Mbars, respectively, according to CALEOS. [It should be emphasized here that we are not suggesting that the damping of rippled shocks is due to the *physical* viscosity of the downstream medium, since accounting for this fluid property lies beyond the Eulerian description adopted in Eq. (12). Thus, while a vibrating string in a viscous liquid is a suggestive simplified model of rippled-shock behavior, it should not be taken too literally in the present context.] In the future, it would be desirable to better elucidate the underlying physical mechanisms and associated EOS characteristics that are responsible for the bifurcated nature of solutions to this class of problems.

The objective of the present investigation was to develop a better understanding of the dynamics of rippled shock fronts in substances with nonideal equations of state. Stated simply, our principal conclusion is that ripple attenuation properties are EOS dependent, and can differ appreciably from those of a perfect gas, even for moderately strong shocks. This result could have important consequences for the realistic modeling of shock-compressed ICF-fuel pellets, since they contain materials whose equations of state are far from ideal (and often poorly understood). Because of their potential for “seeding” hydrodynamic instabilities, a thorough knowledge of how shock ripples evolve during the compression stage of an ICF implosion is crucial for designing successful high-gain targets. The findings of this study represent a significant first step towards this goal. In subsequent investigations, it may be possible to apply the solutions derived herein to understand better the Richtmyer-Meshkov instability [23] for realistic equations of state, or to extend the calculation to incorporate the influence of such effects as convergent geometries, and nonuniform driving mechanisms (e.g., initial target roughness and/or varying laser intensity in the case of direct-drive ICF) that can launch

perturbed shocks [11]. Additionally, a more complete understanding of the dynamics of isolated rippled shocks may be useful in the study of certain type II supernova phenomena [53], and forms the basis for developing a new analytical benchmark to validate the performance of ICF and “high-energy-density physics” codes [17–20].

### ACKNOWLEDGMENTS

This work was performed under the auspices of the U.S. Department of Energy. The author is indebted to Dr. A. L. Velikovich, Dr. A. N. Mostovych, and Professor J. G. Wouchuk for valuable discussions. The assistance of Dr. A. J. Schmitt in the generation of Figs. 6 and 7 is also gratefully acknowledged.

### APPENDIX: LAPLACE TRANSFORMS AND MATHEMATICAL IDENTITIES

We cite in this appendix particular Laplace-transform relations and miscellaneous mathematical identities that were useful in our analysis of the isolated rippled-shock problem. Following convention, we let the symbol  $\mathcal{L}$  represent the Laplace transform of a function  $\Phi(\tau)$ , defined as

$$\mathcal{L}\{\Phi(\tau)\} = \int_0^\infty e^{-s\tau} \Phi(\tau) d\tau \equiv \Phi_L(s), \quad (\text{A1})$$

where the subscript  $L$  is a practical shorthand notation and  $s$  is the Laplace-transform variable. The inverse transform operator is denoted by  $\mathcal{L}^{-1}$ , such that  $\mathcal{L}^{-1}\{\Phi_L(s)\} = \Phi(\tau)$ . In terms of these definitions, the following results can be established [54]:

$$\mathcal{L}\{1\} = 1/s, \quad (\text{A2})$$

$$\mathcal{L}\{J_0(\alpha\tau)\} = 1/\sqrt{s^2 + \alpha^2}, \quad (\text{A3})$$

$$\mathcal{L}\{J_1(\alpha\tau)\} = \alpha^{-1} \left( 1 - \frac{s}{\sqrt{s^2 + \alpha^2}} \right), \quad (\text{A4})$$

$$\mathcal{L} \left\{ \int_0^{\alpha\tau} J_0(w) dw \right\} = \frac{\alpha}{s\sqrt{s^2 + \alpha^2}}, \quad (\text{A5})$$

$$\mathcal{L}^{-1} \left\{ \frac{1}{s + \sqrt{s^2 + \alpha^2}} \right\} = \frac{J_1(\alpha\tau)}{\alpha\tau}, \quad (\text{A6})$$

$$\mathcal{L}^{-1} \left\{ \frac{1}{(s - \mu)^2 + \Omega^2} \right\} = e^{\mu\tau} \frac{\sin \Omega\tau}{\Omega}, \quad (\text{A7})$$

$$\mathcal{L}^{-1} \left\{ \frac{s}{(s - \mu)^2 + \Omega^2} \right\} = e^{\mu\tau} \left( \cos \Omega\tau + \frac{\mu}{\Omega} \sin \Omega\tau \right). \quad (\text{A8})$$

Note that the constants  $\alpha$ ,  $\Omega$ , and  $\mu$  appearing in the equations above are real quantities. An important consequence of Laplace-transform theory is the convolution theorem [41],

which asserts that any two continuous and sufficiently well-behaved functions  $\Phi(\tau)$  and  $\Psi(\tau)$  obey the relation

$$\mathcal{L}^{-1}\{\Phi_L(s)\Psi_L(s)\} = \int_0^\tau \Phi(z)\Psi(\tau-z) dz. \quad (\text{A9})$$

Stated differently, the convolution theorem says that the product  $\Phi_L(s)\Psi_L(s)$  is the Laplace transform of the function defined by the right-hand side of Eq. (A9)—a result that plays a central role in the derivation of the solutions presented in Sec. IV. Other important mathematical identities for this study were [55]

$$\int_0^\infty \frac{J_1(\alpha z)}{\alpha z} \sin \lambda(\tau-z) dz = \begin{cases} \frac{\sqrt{\lambda^2 - \alpha^2} - \lambda}{\alpha^2} \cos \lambda \tau & \text{if } \lambda \geq \alpha \\ \frac{\sqrt{\alpha^2 - \lambda^2}}{\alpha^2} \sin \lambda \tau - \frac{\lambda}{\alpha^2} \cos \lambda \tau & \text{if } \lambda < \alpha, \end{cases} \quad (\text{A10})$$

$$\int_0^\infty \frac{J_1(\alpha z)}{\alpha z} e^{-\sigma z} \cos \alpha z dz = \frac{\{\sqrt{[\sigma^2 + (a-\alpha)^2][\sigma^2 + (a+\alpha)^2]} - a^2 + \sigma^2 + \alpha^2\}^{1/2}}{\sqrt{2}\alpha^2} - \frac{\sigma}{\alpha^2}, \quad (\text{A11})$$

$$\int_0^\infty \frac{J_1(\alpha z)}{\alpha z} e^{-\sigma z} \sin \alpha z dz = -\frac{\{\sqrt{[\sigma^2 + (a-\alpha)^2][\sigma^2 + (a+\alpha)^2]} + a^2 - \sigma^2 - \alpha^2\}^{1/2}}{\sqrt{2}\alpha^2} + \frac{a}{\alpha^2}, \quad (\text{A12})$$

where  $\lambda$ ,  $\sigma$ , and  $a$  are positive real parameters, and the condition  $\alpha > 0$  is assumed in Eq. (A10).

- 
- [1] C.F. McKee and B.T. Draine, *Science* **252**, 397 (1991).  
[2] A. Sasoh and T. Ohara, *J. Phys. Soc. Jpn.* **71**, 2339 (2002).  
[3] See National Technical Information Service Document PB2004-100597 [A. E. Roberts, Los Alamos Scientific Laboratory Report No. LA-299 1945 (unpublished)]. Copies may be ordered from National Technical Information Service, Springfield, VA 22161.  
[4] See National Technical Information Service Document SC-RR-71 0714 [S. L. Thompson and H. S. Lauson, Sandia Laboratories Report No. SC-RR-71-0714 1972 (unpublished)]. Copies may be ordered from National Technical Information Service, Springfield, VA 22161.  
[5] S.P. D'yakov, *Zh. Eksp. Teor. Fiz.* **27**, 288 (1954); Air Force Office of Scientific Research Report No. AFOSR-TN-56-406, 1956 (unpublished).  
[6] S. Eliezer, A. Ghatak, and H. Hora, *Fundamentals of Equation of State* (World Scientific, Singapore, 2002).  
[7] J.J. Duderstadt and G. A. Moses, *Inertial Confinement Fusion* (Wiley, New York, 1982).  
[8] J.D. Lindl, *Inertial Confinement Fusion* (Springer-Verlag, New York, 1998).  
[9] J.O. Kane, H.F. Robey, B.A. Remington, R.P. Drake, J. Knauer, D.D. Ryutov, H. Louis, R. Teyssier, O. Hurricane, D. Arnett, R. Rosner, and A. Calder, *Phys. Rev. E* **63**, 055401 (2001).  
[10] S. Eliezer, *The Interaction of High-Power Lasers with Plasmas* (IOP Publishing, Bristol, 2002).  
[11] R. Ishizaki and K. Nishihara, *Phys. Rev. Lett.* **78**, 1920 (1997).  
[12] T. Endo, K. Shigemori, H. Azechi, A. Nishiguchi, K. Mima, M. Sato, M. Nakai, S. Nakaji, N. Miyanaga, S. Matsuoka, A. Ando, K.A. Tanaka, and S. Nakai, *Phys. Rev. Lett.* **74**, 3608 (1995).  
[13] G. Fraley, *Phys. Fluids* **29**, 376 (1986).  
[14] N.C. Freeman, *Proc. R. Soc. London, Ser. A* **228**, 341 (1955).  
[15] P.M. Zaidel, *J. Appl. Math. Mech.* **24**, 316 (1960).  
[16] M.G. Briscoe and A.A. Kovitz, *J. Fluid Mech.* **31**, 529 (1968).  
[17] G. Zimmerman, D. Kershaw, D. Bailey, and J. Harte, *J. Opt. Soc. Am.* **68**, 549 (1978).  
[18] M.H. Emery, J.H. Gardner, and J.P. Boris, *Appl. Phys. Lett.* **41**, 808 (1982).  
[19] See National Technical Information Service Document DE-96004569 [M. M. Marinak, R. E. Tipton, B. A. Remington, S. W. Haan, and S. V. Weber, ICF Quarterly Report UCRL-LR-105821-95-3, 1995 (unpublished)]. Copies may be ordered from National Technical Information Service, Springfield, VA 22161.  
[20] R.R. Peterson, J.J. Macfarlane, J.F. Santarius, P. Wang, and G.A. Moses, *Fusion Technol.* **30**, 783 (1996).  
[21] J.H. Gardner, A.J. Schmitt, J.P. Dahlburg, C.J. Pawley, S.E. Bodner, S.P. Obenschain, V. Serlin, and Y. Aglitskiy, *Phys. Plasmas* **5**, 1935 (1998).  
[22] S. Chandrasekhar, *Hydrodynamic and Hydromagnetic Stability* (Oxford University, Oxford, 1961).  
[23] R.D. Richtmyer, *Commun. Pure Appl. Math.* **13**, 297 (1960); E.E. Meshkov, *Fluid Dyn.* **4**, 101 (5) (1969).  
[24] D. Munro, *Phys. Fluids B* **1**, 134 (1989).  
[25] L.D. Landau and E.M. Lifshitz, *Fluid Mechanics*, 2nd ed. (Pergamon, Oxford, 1987).  
[26] See National Technical Information Service Document DE-94011699 [J.D. Johnson, Los Alamos National Laboratory Report No. LA-UR-94-1451, 1994 (unpublished)]. Copies may be ordered from National Technical Information Service, Springfield, VA 22161.  
[27] R.M. More, K.H. Warren, D.A. Young, and G.B. Zimmerman, *Phys. Fluids* **31**, 3059 (1988).

- [28] L.V. Altshuler, S.B. Korner, A.A. Bakanova, and R.F. Trunin, Zh. Eksp. Teor. Fiz. **38**, 790 (1960) [Sov. Phys. JETP **11**, 573 (1960)].
- [29] Y. B. Zel'dovich and Y. P. Raizer, *Physics of Shock Waves and High-Temperature Hydrodynamic Phenomena* (Dover, New York, 2002).
- [30] G.R. Fowles and G.W. Swan, Phys. Rev. Lett. **30**, 1023 (1973).
- [31] N.M. Kuznetsov, Usp. Fiz. Nauk **159**, 493 (1989) [Sov. Phys. Usp. **32**, 993 (1989)].
- [32] G. Joulain and P. Vidal, *Hydrodynamics and Nonlinear Instabilities* (Cambridge University, Cambridge, 1998), p. 614.
- [33] See National Technical Information Service Document PB2004-100598 [H. Bethe, Office of Scientific Research and Development Report No. 445, 1942 (unpublished)]. Copies may be ordered from National Technical Information Service, Springfield, VA 22161.
- [34] G.E. Duvall and R.A. Graham, Rev. Mod. Phys. **49**, 523 (1977).
- [35] C.S. Gardner, Phys. Fluids **6**, 1367 (1963).
- [36] J. Lighthill, *Waves in Fluids* (Cambridge University, Cambridge, 1993).
- [37] G. Kane, *Modern Elementary Particle Physics* (Addison-Wesley, Redwood City, CA, 1987).
- [38] P.M. Morse and H. Feshbach, *Methods of Theoretical Physics* (McGraw-Hill, New York, 1953), p. 139.
- [39] F.B. Hildebrand, *Advanced Calculus for Application* (Prentice-Hall, New York, 1976).
- [40] K.R. Symon, *Mechanics* (Addison-Wesley, Reading, MA, 1971).
- [41] G. Arfken, *Mathematical Methods for Physicists* (Academic, San Diego, 1985).
- [42] V.M. Kontorovich, Zh. Eksp. Teor. Fiz. **33**, 1525 (1957) [Sov. Phys. JETP **6**, 1179 (1957)].
- [43] G.R. Fowles, Phys. Fluids **24**, 220 (1981).
- [44] N.M. Kuznetsov, Zh. Eksp. Teor. Fiz. **93**, 1986 (1987) [Sov. Phys. JETP **66**, 1132 (1987)].
- [45] J.W. Bates and D.C. Montgomery, Phys. Rev. Lett. **84**, 1180 (2000).
- [46] K.C. Lapworth, J. Fluid Mech. **2**, 341 (1957).
- [47] J.P. Boris and D.L. Book, J. Comput. Phys. **11**, 38 (1973); see also *Methods in Computational Physics* (Academic, New York, 1976), Vol. 16, pp. 85–129.
- [48] P.M. Morse and K.U. Ingard, *Theoretical Acoustics* (Princeton University, Princeton, 1986).
- [49] R.B. Lindsay, *Mechanical Radiation* (McGraw-Hill, New York, 1960).
- [50] F. Reif, *Fundamentals of Statistical and Thermal Physics* (McGraw-Hill, New York, 1965).
- [51] H.S. Green, *The Molecular Theory of Fluids* (Dover, New York, 1960).
- [52] D.L. Goodstein, *States of Matter* (Prentice-Hall, Englewood Cliffs, 1975).
- [53] G. Bazan and D. Arnett, Astrophys. J. **496**, 316 (1998).
- [54] M. Abramowitz and I. A. Stegun, *Handbook of Mathematical Functions* (Dover, New York, 1972).
- [55] I.S. Gradshteyn and I.M. Ryzhik, *Tables of Integrals, Series, and Products* (Academic, San Diego, 1980).